Thomas, H. R. & Rees, S. W. (2009). *Géotechnique* **59**, No. 4, 365–375 [**doi:** 10.1680/geot.2008.59.4.365]

Measured and simulated heat transfer to foundation soils

H. R. THOMAS* and S. W. REES*

The drive towards energy-efficient, low-carbon buildings is a clear priority for many countries. Furthermore, ground heat transfer is understood to play an important role in the overall thermal performance of buildings. This paper presents the results of an in-depth investigation of heat transfer from buildings to the ground. The research involved in situ measurements of heat transfer to the ground from full-scale buildings. The results have been utilised to help develop and validate suitable predictive tools to aid thermal design. Numerical simulations have been undertaken that reveal the transient form of energy losses from typical buildings to the ground over a seasonal time frame. Comparisons are made between numerical results and measured data over an annual cycle. Overall, good correlation of results has been achieved. The thermal properties of foundation soils are known to be dependent on water content. A preliminary assessment of the significance of this aspect of the problem is also considered. In particular, it has been shown that an increase in soil moisture content may cause an increase in heat flux of over 20% for a two-dimensional test case. In summary, innovative low-energy sustainable design is receiving increasing attention. The current work will contribute to this overall objective by ensuring that adequate attention is given to subsurface heat transfer.

KEYWORDS: monitoring; numerical modelling; temperature effects

La poussée actuelle vers la réalisation de bâtiments à consommation énergétique limitée et à faibles émissions de CO_2 est, dans de nombreux pays, une priorité bien définie. En outre, les transferts thermiques avec le sol semblent jouer un rôle important dans la performance thermique des bâtiments. La présente communication présente les résultats d'une recherche en profondeur sur le transfert thermique des bâtiments au sol. Cette recherche a comporté l'exécution de mesures in situ du transfert thermique de bâtiments grandeur nature dans le sol : on a utilisé les résultats pour la création et la validité d'outils prédictifs appropriés, afin de faciliter l'étude thermique. On a également entrepris des simulations numériques, qui révèlent la forme transitoire des pertes d'énergie de bâtiments typiques dans le sol, dans le cadre d'une saison. On effectue des comparaisons entre les résultats numériques et des données mesurées dans le cadre d'une année. Dans l'ensemble, on obtient une bonne corrélation entre les résultats. On sait que les propriétés thermiques des sols de fondation sont tributaires de la teneur en eau, et on se penche également sur une évaluation préliminaire de l'importance de cet aspect du problème. On démontre en particulier qu'une augmentation de la teneur en humidité du sol risque d'accroître de plus de 20% le flux thermique dans un cas d'essai bidimensionnel. En résumé, les créations innovantes soutenables avec faible consommation d'énergie font l'objet d'un intérêt croissant. Les travaux en cours contribueront à la réalisation de cet objectif général, en assurant que l'on attache une importance suffisante au transfert thermique sub-surface.

INTRODUCTION

The drive towards urban sustainability underpins much UK policy on energy efficiency in the built environment. For example, Banfill & Peacock (2007) provide a useful critique of recent proposals by the UK government to require new housing to become progressively more energy efficient, leading to net zero carbon dioxide emissions from 2016. Related developments in the UK Building Regulations are discussed by Meacham *et al.* (2005).

The UK government has set a domestic target to reduce carbon dioxide emissions by 20% below 1990 levels by 2010. One of numerous related initiatives detailed in *Climate Change: The UK Programme 2006* (Defra, 2006) is The Low Carbon Buildings Programme (LCBP). This programme aims to mark a change from previous grant programmes by taking a more holistic approach to reducing carbon emissions. The objective is to promote innovative combinations of energy efficiency and microgeneration technologies. A budget of £80 million has been allocated over the period 2006 to 2009 for this purpose.

Manuscript received 29 April 2008; revised manuscript accepted 8 December 2008.
Discussion on this paper closes on 1 October 2009, for further details see p. ii.
* Geoenvironmental Engineering Research Centre, Cardiff School of Engineering, Cardiff, UK.

Across Europe there are currently some 160 million buildings that together account for over 40% of total energy usage. This energy is primarily used to achieve adequate standards of heating, ventilation and air conditioning. In addition, over 40% of European Union (EU) carbon dioxide emissions can be attributed to the building stock, and the proportion is increasing. Lowe (2007) provides a clear indication of the impetus that now exists to try and improve the position. Within the last two years, several key strategic publications have appeared. These include, for example

(*a*) the EU Action Plan for Energy Efficiency (CEC, 2006)
(*b*) the Stern Review (Stern, 2006)
(*c*) the Fourth Assessment Report of the Intergovernmental Panel on Climate Change (IPCC) (IPCC, 2007).

The EU Action Plan for Energy Efficiency aims to achieve a 20% energy saving by 2020. The EU's specific proposals for buildings are more ambitious, with planned savings of 28%.

It is therefore clear that energy-efficient design of buildings now, more than ever, requires careful consideration of the thermodynamic response of the entire building. It is well established that the earth-contact elements of a building also play a significant role in the overall thermal performance. Al-Ajmi *et al.* (2006), Kumar *et al.* (2007) and Zhong & Braun (2007) provide some recent developments in the simulation of ground heat transfer in relation to floor slabs, whereas Krarti (2004a, 2004b) considers a more complex

ground heat transfer in relation to the analysis of heat and moisture transfer beneath freezer foundations. Although the application considered by Krarti is quite specific, the formulation involved is more widely applicable. Cui *et al.* (2005) provide useful information on the determination of thermal and hydraulic soil properties. Their work focuses on field simulation of in situ water content and temperature changes due to ground–atmospheric interactions.

Ground heat transfer is also increasingly important within emerging technologies. For example, Brandl (2006) provides an excellent treatise on thermo-active ground structures. Design and construction are considered in detail, with examples given (among others) of energy piles, thermo-active concrete slabs and a thermo-active traffic tunnel. The underlying principles require an understanding of ground heat transfer, coupled with clear utilisation of the thermal mass of the structural elements involved. In a similar manner, Underwood (2007) presents recent research on the design and performance of ground-source heat pumps and ground-sink cooling systems using vertical borehole arrays for commercial applications in the UK. The results show that, in some circumstances, a substantial reduction in energy (and hence in carbon) of up to and exceeding 50% can be expected when using ground-source heat pumps for winter heating.

The current paper builds on the outcome of a research programme undertaken at Cardiff University (Rees & Thomas, 1997), funded by the Engineering and Physical Sciences Research Council (EPSRC). The overall thrust of the work relates to development and validation of ground heat transfer models. In the work presented here, two full-scale monitoring experiments are summarised and then used to reveal heat loss patterns from buildings to the ground. The first dataset was obtained at Cardiff University (Thomas & Rees, 1998); the second dataset was obtained, by others, at Sendai University, Japan (Hasegawa *et al.*, 1987; Yoshino *et al.*, 1990, 1992; Sobotka *et al.*, 1995).

It is generally recognised that there is a limited amount of robust field data available in this research area. The shortage of such data not only limits our understanding of the real thermal response of buildings but also inhibits the validation of predictive numerical models. This paper addresses some of these topical issues by presenting comprehensive field data.

Various design guides exist that, to some extent, account for heat transfer through the earth-contact elements of a building. Application of these procedures for the experimental data considered here has been undertaken previously (Adjali *et al.*, 2004). In particular, Adjali *et al.* considered application of the four main design guides,

(*a*) the American Society of Heating, Refrigerating and Air-conditioning Engineers (ASHRAE, 1993)
(*b*) the UK guide from the Chartered Institution of Building Services Engineers (CIBSE, 1986)
(*c*) the French guide from the Association des Ingénieurs de Climatisation et de Ventilation de France (AICVF, 1990)
(*d*) the European guide from the European Committee for Standardisation (CEN/TC 89, 1992).

Results were found to vary significantly from guide to guide. Detailed consideration of the various advantages and disadvantages of each method was also provided. This work is viewed as a useful companion paper to the current contribution.

THEORETICAL AND NUMERICAL CONSIDERATIONS

Heat transfer may take place by way of conduction, convection or radiation. In practice, for many soils, heat transfer by conduction is clearly the most significant process (Rees *et al.*, 2000). Therefore convection and radiation are excluded from consideration here. From conservation of energy across a small control element it is possible to derive various forms of the heat conduction equation (Lewis *et al.*, 1996). For example, the heat flux through a two-dimensional Cartesian domain is described by

$$\boldsymbol{q} = \lambda\left(\frac{\partial T}{\partial x}\boldsymbol{i} + \frac{\partial T}{\partial z}\boldsymbol{j}\right) \tag{1}$$

where λ is the thermal conductivity of the material, $\boldsymbol{i}$ and $\boldsymbol{j}$ are unit vectors in the x and z directions, $\boldsymbol{q}$ is the heat flux vector and T is temperature. Then the steady-state heat conduction equation for an isotropic material can be written as

$$\lambda\left(\frac{\partial^2 T}{\partial x^2} + \frac{\partial^2 T}{\partial z^2}\right) = 0 \tag{2}$$

For transient problems, in the absence of heat generation within the medium, the governing two-dimensional form of the heat conduction equation is

$$\lambda\left(\frac{\partial^2 T}{\partial x^2} + \frac{\partial^2 T}{\partial z^2}\right) = \rho c\frac{\partial T}{\partial t} \tag{3}$$

where ρ is density and c is specific heat.

The work presented here is based on the use of in-house finite element software to solve the relevant heat conduction equations. In particular, a numerical solution is achieved using the Galerkin weighted residual approach for spatial discretisation coupled with a finite difference time-marching scheme. The corresponding discrete equations may be summarised as

$$\boldsymbol{K}\boldsymbol{T} + \boldsymbol{C}\boldsymbol{T} = \boldsymbol{f} \tag{4}$$

where

$$\boldsymbol{K} = \int_{\Omega} \lambda\nabla N_i \nabla N_j \mathrm{d}x\mathrm{d}z \tag{5}$$

$$\boldsymbol{C} = \int_{\Omega} CN_i N_j \mathrm{d}x\mathrm{d}z \tag{6}$$

$$\boldsymbol{f} = \int_{\Gamma} N_i \pi \mathrm{d}\Gamma \tag{7}$$

$$\boldsymbol{T} = \frac{\partial \boldsymbol{T}}{\partial t} \tag{8}$$

where Ω and Γ refer to the domain and the boundary respectively; π is the flux on the boundary, and N_i and N_j are the shape functions. $\boldsymbol{T}$ is the vector of unknown nodal temperatures, and C is the volumetric heat capacity ($= \rho c$). Standard eight-node isoparametric elements have been employed (Lewis *et al.*, 1996).

Application of the resulting numerical model requires specification of the thermal conductivity and (for transient problems) the volumetric heat capacity. To this end, there are various models available for the calculation of the thermal conductivity of the granular materials (Rees *et al.*, 2000; Tang *et al.*, 2008). Comparisons between the measured and calculated thermal conductivity values using several models can be found in the literature (Woodside & Messmer, 1961; Farouki, 1982). None of these models can be used to predict the thermal conductivity accurately for all soil types, or for the full range of moisture content. Even for a limited range of application, predictions have been shown to deviate considerably from experimental data. However, the geometric mean equation has been found to be adequate by

several researchers (Sass *et al.*, 1971; Bloomer, 1981), and is therefore used in this work. A brief description of the method follows.

In the geometric mean approach, the overall (bulk) soil thermal conductivity can be determined from

$$\lambda = \prod_{i=1}^{3} \lambda_i^{\chi_i} \tag{9}$$

where λ_i represents the corresponding thermal conductivities of the solid, water and air components of the soil, and χ_i represents the corresponding volume fractions. (Here Π is used in the traditional sense to imply product terms.) The volume fractions in equation (9) can be calculated from the expressions

$$\chi_s = 1 - \eta \tag{10}$$

$$\chi_w = \eta S_r \tag{11}$$

$$\chi_a = \eta(1 - S_r) \tag{12}$$

where η is the porosity of the soil, S_r is the degree of saturation, and χ_s, χ_w and χ_a denote the volume fractions of three constituents of soil: solid, water and air. It is therefore clear that, within this framework, the thermal conductivity of the soil is implicitly dependent on the degree of saturation (or moisture content) of the soil.

The heat capacity of a material is required when non-steady solutions are to be determined. In effect, the heat capacity defines the amount of energy stored in a material per unit mass per unit change in temperature (SI units J/kg K). It is often satisfactory to calculate the volumetric heat capacity of soils by adding the heat capacities of the different constituents according to their volume fraction,

$$C = \chi_s \rho_s c_s + \chi_w \rho_w c_w + \chi_a \rho_a c_a \tag{13}$$

where c_s, c_w and c_a are the specific heat capacities of the three soil constituents respectively (solid, water and air), and ρ_s, ρ_w and ρ_a are the respective densities. The heat capacity of a soil having more than three constituents can be calculated by simply adding more terms into equation (13).

Table 1 provides some relevant thermal properties. It is evident from this information that the thermal conductivity of water is much greater than that of air. Thus the degree of saturation of a soil can be expected to have a significant influence on its bulk thermal conductivity. It is also evident that the thermal conductivity of various solid minerals can be very high, with values of quartz at over 8 W/m K.

MEASUREMENT AND SIMULATION OF GROUND HEAT TRANSFER

Case study 1: The West Building, Cardiff University, UK

In situ measurement. The construction of a new building at the site of the Cardiff School of Engineering provided an opportunity to conduct an in situ experimental investigation of heat losses through the floor slabs of the building to the foundation soils beneath. The investigation was supported by EPSRC (formerly SERC), and the raw data collected have been presented in some detail previously (Thomas & Rees, 1998). The West Building is typical of modern commercial construction, and comprises a steel frame with two composite suspended floors and a concrete ground floor slab, 150 mm thick, on 600 mm of hardcore.

Table 1. Some typical thermal properties of soils (De Vries, 1966)

Substance	Thermal conductivity: W/m K	Specific heat: W/m^3 K	Density: kg/m^3
Quartz	8·79	2010	2660
Clay minerals	2·93	2010	2650
Organic matter	0·25	2512	1300
Water	0·57	4186	1000
Ice	2·18	1884	920
Air	0·025	1·256	1·25

Note: These values have been converted to SI units from the original reference.

Site investigation revealed the soil profile to a depth of 11·5 m below the floor foundation level. Borehole logs recorded approximately 3 m of made ground immediately below the original surface level. Much of the made ground was removed prior to construction. The remaining foundation soils listed from the foundation layer downwards include approximately 2·5 m of black silty clay, 2·19 m of sand gravel and boulders, and red-brown silty clay turning to fractured mudstone at depth.

A cross-section through one of the floor slabs, indicating the range of instrumentation employed, is shown in Fig. 1. The acronyms employed in the figure are HFS for heat flux sensors, TC for thermocouples, TS for ground temperature sensors, NP for neutron probe access tubes, and TP for thermal probe measurement locations. Details of the precise instrumentation used have been provided by Thomas & Rees (1998).

The experiment was designed to reveal the transient nature of the thermal behaviour of the site. It was therefore necessary to obtain data at relatively short time intervals. This was achieved by automated electronic interrogation of some 152 instruments at 30 min intervals. Neutron probe, thermal probe and piezometric readings were collected manually on a weekly basis. Over the duration (approximately 2 years) of the monitoring exercise, some 4·1 million readings were recorded, processed and stored.

Figure 2 shows the measured internal and external daily average temperatures recorded at the site. The data shown span a continuous period, starting from 19 September (0 days) and ending on 23 July (309 days). Internal temperatures were maintained at around 20°C, whereas external temperatures followed a typical seasonal variation, ranging from winter lows of around −3°C to summer highs of approximately 23°C. These data are daily averages: the diurnal variation showed greater temperature fluctuation.

Figure 3 presents the ground temperature variation recorded at four temperature sensor locations. TS1 and TS4 are located in stack 1 (directly beneath the floor slab) at depths of 0·25 m and 1·0 m respectively. TS56 and TS59 are located in stack 3 (remote from the building), again at depths of 0·25 m and 1·0 m respectively. The results reveal that there is a significant difference between the ground temperature variations recorded at the internal stacks and those recorded at the external stack. In general, the results show that the range of seasonal variation in ground temperature decreases as the depth below the ground surface increases. Furthermore, the influence of short-term climatic temperature variations is clearly reflected in the near-surface temperature variation (TS56, 0·25 m depth). This effect is much reduced at 1·0 m depth, and was found to be negligible at 3·00 m depth.

Material properties. Characterisation of the thermal properties at the Cardiff experiment has been dealt with elsewhere (Thomas & Rees, 1998), and will therefore not be considered in any further detail here. However, for completeness, the resulting specification of the thermal properties that are employed in the following simulation is given in Table 2.

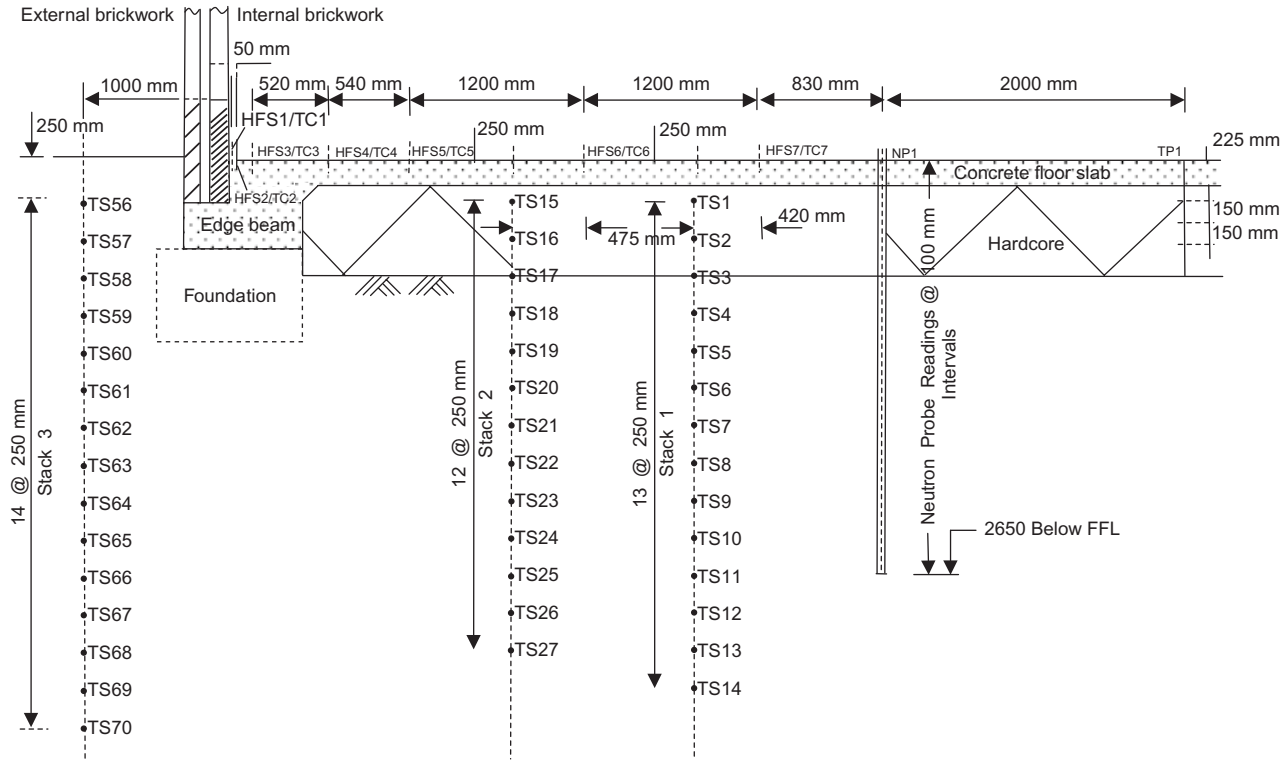

Fig. 1. Cardiff experimental layout: TS, temperature sensor; NP, neutron probe; HFS, heat flux sensor; FFL, finished floor level

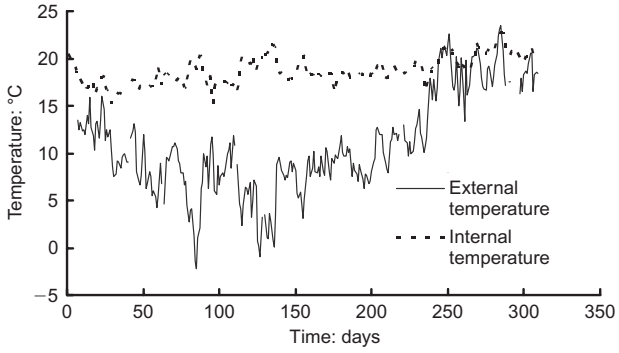

Fig. 2. Cardiff data: internal and external air temperature

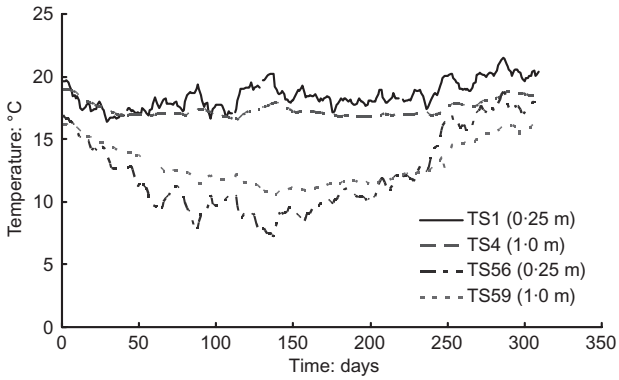

Fig. 3. Cardiff data: ground temperature variations

Table 2. Thermal properties: Cardiff experiment (Thomas & Rees, 1998)

Material	Thermal conductivity: W/m K	Specific heat capacity: J/kg K	Density: kg/m^3
Concrete	1·37	880	2400
Hardcore	2·22	930	2000
Made ground	1·5	2000	1500
Sand and gravel	2·0	1350	1500
Cavity wall*	0·397	853	994

*Overall value based on brick/air/block thicknesses.

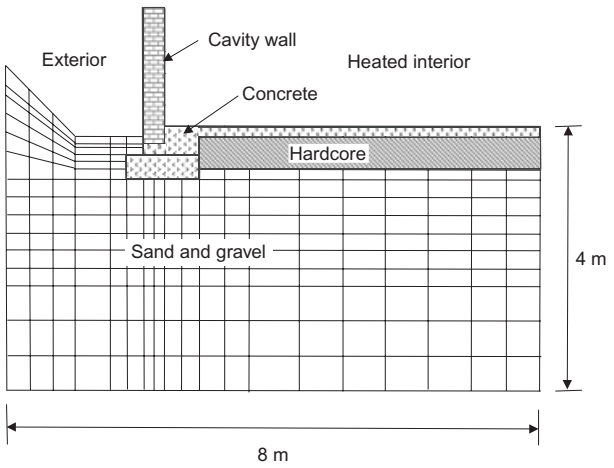

Fig. 4. Cardiff experiment: finite element discretisation

Numerical simulation. Remote from the corners of the building, the experimental results indicated that a two-dimensional simulation may be adequate. The example considered here therefore focuses on a two-dimensional domain, as shown in Fig. 4. The finite element mesh used for the analysis consists of 327 quadrilateral elements and 1070 nodes. A timestep size of 21 600 s was used. This level of discretisation was found, via preliminary studies, to provide spatially and temporally converged results.

Boundary conditions for the problem were determined directly from the measured data. In particular, the mean daily temperatures have been used directly in the form of fixed (Dirichlet type) boundary conditions. As discussed above, it is clear that there is a spatial variation in temperature within the room, in addition to the temporal variation through the seasons. The temporal variation is readily accommodated in the model in the form of time-varying fixed boundary conditions. A series of such 'time curves', each pertaining to a distinct region of the floor slab surface, also allows the spatial variation to be accommodated in an approximate manner. The outside temperature variation is also included within the simulation as a separate set of time-varying fixed boundary conditions applied to nodes lying on the external surface of the domain.

Determination of the initial temperature distribution throughout the two-dimensional domain under consideration is complicated by the fact that experimental data were available only at the precise locations of the three temperature sensor stacks, as shown in Fig. 1. Therefore it is clear that some form of interpolation or initialisation is necessary to define the temperature variation throughout the domain. In this case, a preliminary analysis was performed using the numerical model itself to help establish a realistic initial distribution of temperature. Based on the experimental readings, this was achieved by running the model using an indoor surface temperature of 20°C and an outdoor surface temperature of 13·5°C (each applied as constant Dirichlet boundary condition). In addition, internal nodes located at the same positions as the temperature sensors were also prescribed at the recorded initial temperature values. All other regions of the domain were free to vary from an arbitrary initial temperature of 18°C. The preliminary analysis was run until a steady-state condition was achieved.

Figure 5 shows an example of the transient results beneath the floor slab of the building. In particular, the results are for a position at a depth of 0·25 m (TS1, stack 1, Fig. 1). The numerical approach, utilising time-varying surface boundaries, has produced results that are in very good agreement with the measured data at this position. In general, at this location, the greatest variation in temperature occurred near the surface of the ground floor slab, and progressively reduced with depth. The model was also capable of reproducing this aspect of field behaviour.

Figure 6 shows the results obtained in the ground adjacent to the building (TS56, stack 3, Fig. 1). At this location, the influence of the external air temperature variation is more pronounced. However, a reasonable match between the simulated and measured data has still been achieved. Temperature variations reduced as the depth below the ground surface increased. At 3·0 m depth relatively little variation was observed in either the experimental or numerical results.

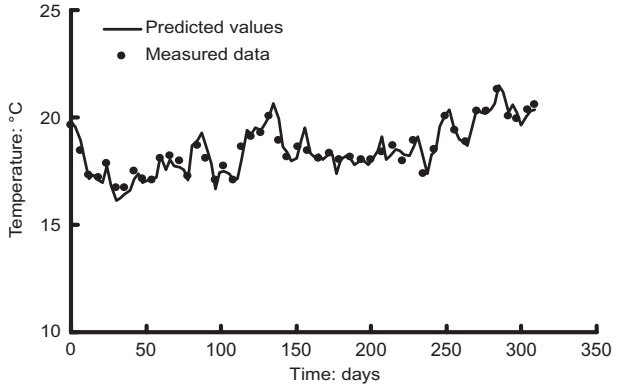

Fig. 5. Measured and simulated ground temperatures: stack 1, TS1

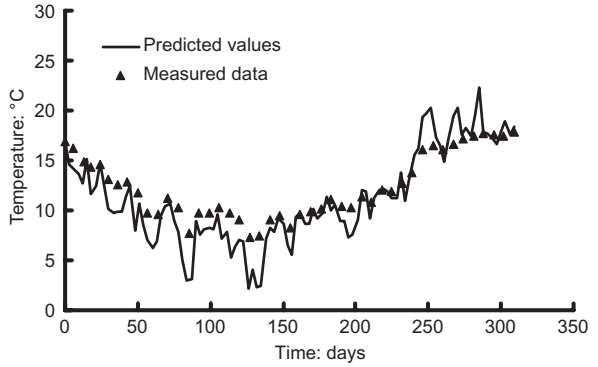

Fig. 6. Measured and simulated ground temperatures: stack 3, TS56

Case study 2: The Japanese test house experiment, Sendai, Japan

In situ measurement. The measured data briefly described here were recorded (by others) at Tohoku University, Sendai, Japan (Hasegawa *et al.*, 1987; Yoshino *et al.*, 1990; Yoshino *et al.*, 1992; Sobotka *et al.*, 1995). The experiment involved the design and construction of a full-scale, two-room test-house. An east–west cross-section of the test house is shown in Fig. 7. The floor level is 1·3 m below the ground surface. The floor of the corridor was insulated on its upper and lower surfaces. Horizontal edge insulation, 1·35 m wide and 0·2 m thick, surrounded room D and was placed at 0·3 m below the ground surface.

The rooms were of square vertical cross-section, approximately 2·7 m by 2·7 m, and were 5·4 m long. The below-ground part of the test house was made using a concrete with a thermal conductivity of 1·66 W/m K. The walls had a thickness of 0·2 m and the floor was 0·3 m thick. The side walls above the ground surface, the internal walls facing the corridor and the ceilings of each room had 0·2 m foam polystyrene insulation (thermal conductivity 0·04 W/m K). Each room had a south-facing double-glazed window.

All construction gaps in the building envelope were filled with sealing materials. The test rooms were described as being so airtight that their thermal performance was not influenced by air leakage. There were no ventilation systems within the test house. Room temperatures were thermostatically controlled via an electric space heater. The soil was thought to be quite uniform, and was found to have a thermal conductivity of 0·99 W/m K.

Figure 8 shows the average-daily measured internal and external temperature variation. The results are presented for a continuous one-year period, with Day 0 occurring on 1 January. Internal temperature regulation held the room at approximately 20°C for the first 200 days, when external temperatures were generally low. The temperature regulation was not as effective (in terms of comfort) during the summer period.

Figure 9 presents a selection of ground temperature variations measured during the experiment. Sensors C68, C67, C66 and C65 are in the foundation soil located beneath Room D. Sensor C65 was position at the slab/soil interface. Sensor C68 was approximately 3·2 m below the lower surface of the floor slab. A clear variation with depth can be seen. Sensor C41 was located 0·3 m below the ground surface, just adjacent to the building. Here the influence of the external air temperature variation is much more pronounced.

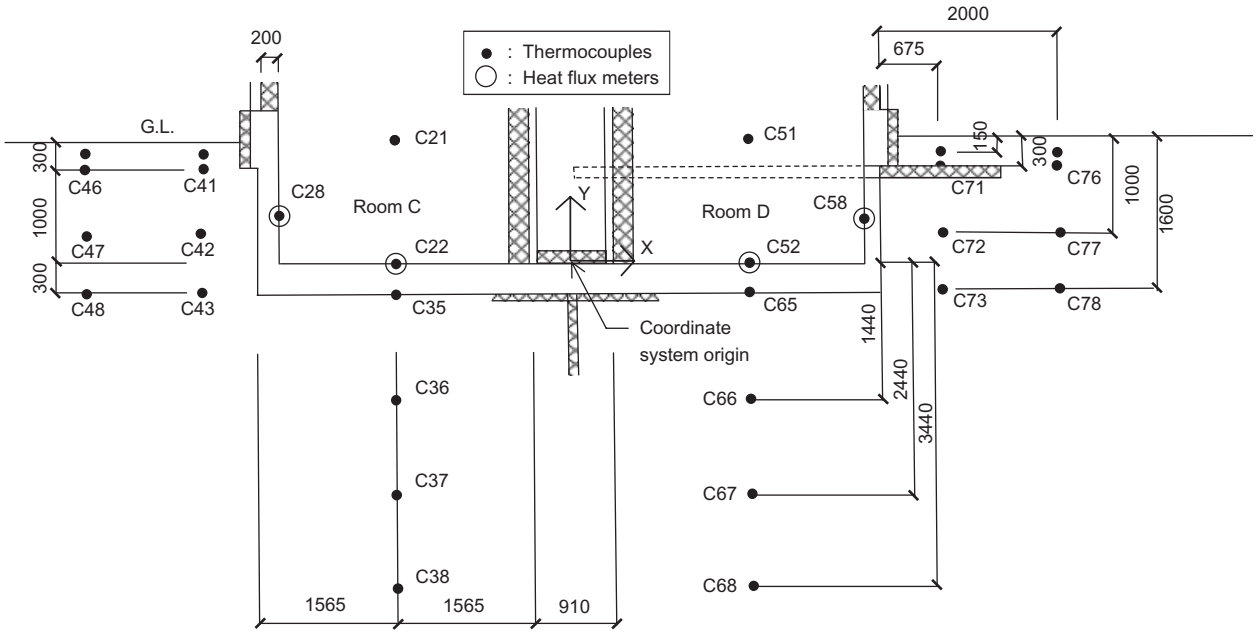

Fig. 7. Japanese test house experimental layout: C: thermocouple channel numbers; G.L.: ground level. All dimensions in mm

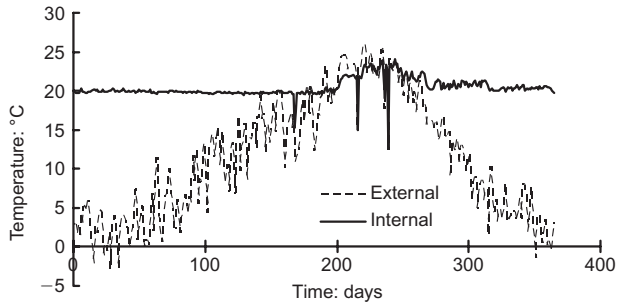

Fig. 8. Japanese test house: internal and external air temperatures

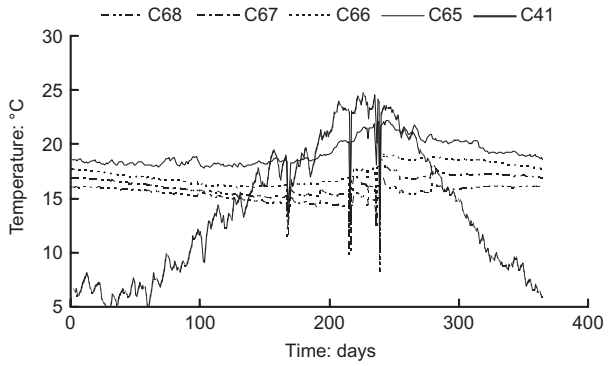

Fig. 9. Japanese test house: ground temperature variations

Material properties. In order to simplify the finite element discretisation of the field problem, lumped material properties were used in some locations. In particular, the zones of concrete and side wall insulation and the zones of concrete and insulation on the corridor floor were represented by composite thermal properties. Woodside & Messmer (1961) provided a simple approach for this purpose. De Vries's (1966) approach for geometric averaging of the heat capacity and density of the composite materials was used to estimate the specific heat capacity and density of the combined materials. Thermal properties of the soil were not directly measured during the field experiment. However, Sobotka *et al.* (1995) performed a numerical sensitivity study of the problem that suggested that the thermal conductivity of the soil was likely to be around 0·99 W/m K. In summary, the thermal properties used in this case study are presented in Table 3 (after Yoshino *et al.*, 1990).

Numerical simulation. Since room D (only) was surrounded by an insulation strip, thermal symmetry between the two rooms did not exist. Therefore both rooms were included in the two-dimensional finite element representation of the east–west cross-section through the experiment shown in Fig. 10. The overall dimensions of the domain are approximately 30 m width by 10 m depth. Preliminary analyses of the problem were undertaken to ensure that these dimensions were sufficiently remote to ensure that the 'far-field' boundary conditions applied had little influence on the results obtained in the region of interest.

Determination of the initial and boundary conditions was

Table 3. Thermal properties: Japanese test house experiment (Yoshino *et al.*, 1990)

Material	Thermal conductivity, λ: W/m K	Specific heat capacity, Cp: J/kg K	Density, ρ: kg/m
Soil	0·990	1435	1600
Concrete	1·630	800	2200
Concrete + insulation (side wall)	0·096	1146	1326
Concrete + insulation (corridor)	0·146	1016	1654
Insulation	0·040	1666	15

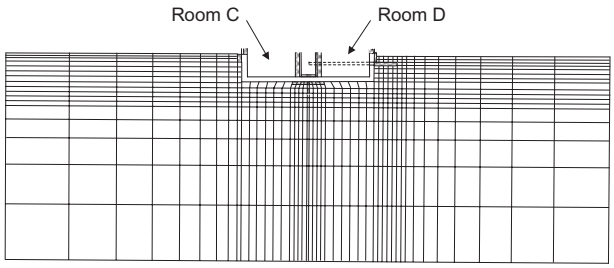

Fig. 10. Japanese test house: finite element discretisation

achieved in a similar manner to that described above for the Cardiff experiment. The internal and external temperature variations shown in Fig. 8 effectively defined the boundary conditions employed here. In the absence of any measured data at 10 m below ground surface, the lower boundary of the domain was fixed at a temperature of 12°C (i.e. the average outdoor air temperature). The vertical boundaries remote from the test house were assumed to be adiabatic.

Figure 11 presents a comparison of numerical and experimental results at the location of sensor C66 (see Fig. 7). Overall, a good correlation between results has been achieved. The experimental data are shown as discrete data points in the figure, and some instability in the instrumentation is apparent. However, the overall trends remain, and no attempt has been made here to eliminate the small number of suspect data points.

Figure 12 shows the results achieved near the ground surface adjacent to the building (sensor C41). The external climate variation has caused a much greater temperature variation than that beneath the building. The numerical simulation is also in very good agreement with the measured data at this location.

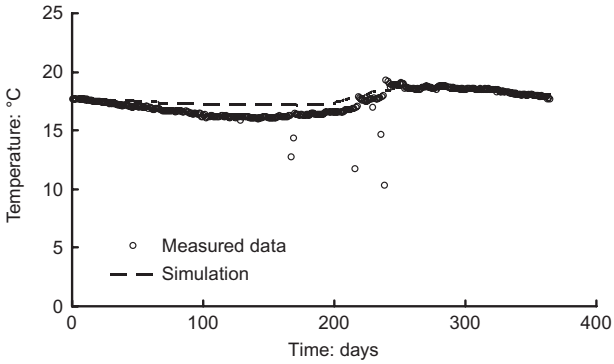

Fig. 11. Measured and simulated ground temperatures: Channel C66

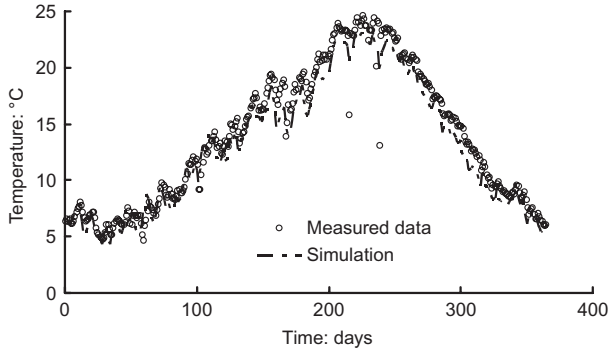

Fig. 12. Measured and simulated ground temperatures: Channel C41

INFLUENCE OF SOIL MOISTURE CONTENT ON HEAT TRANSFER

Reference back to Table 1 indicates that the thermal conductivity of water is at least 20 times greater than that of air. Therefore the degree of saturation of a soil can be expected to have a significant influence on its overall (bulk) thermal conductivity. In the UK, the depth of the water table can vary spatially, depending on local conditions (soil profile, surface topography, cover, runoff/on etc.), and can vary seasonally, depending on climatic conditions (precipitation, evaporation, evapotranspiration). In view of these factors, research has been undertaken to assess how changes in moisture content caused by a variation in the position of the water table are likely to affect (a) the thermal conductivity of the soil in this zone, and (b) the corresponding heat loss to the ground. Two steady-state ground heat transfer problems have been designed for this purpose. The first is a simple one-dimensional problem; the second represents two-dimensional conditions relevant to the case studies considered above.

In these test problems the moisture content profile above the water table is assumed to be in gravitational equilibrium. The groundwater beneath the water table is assumed to be static (zero flow rate). This assumption is thought to be a reasonable starting point, since many soils have a very low permeability. Therefore no attempt is made here to include the effect of heat transfer that may occur because of convection. The resulting static profile in soil moisture content has been recalculated for a variety of water table depths. This information is then used to calculate a depth variation in soil thermal conductivity, which, in turn, is employed in steady-state heat conduction analyses of the test problems. The approach adopted therefore involves two separate (uncoupled) stages.

It is recognised that, in reality, heat and moisture transfer will occur as a coupled process. For example, heat transfer to the bulk movement of liquid, vapour flow, phase change and sensible heat transfer can be included where appropriate. Within the context of the current work, Janssen *et al.* (2004) provide a useful assessment of the significance of coupling. Their work demonstrates that up to 11% difference between a linear (uncoupled) and non-linear (coupled) simulation can occur for this class of problem. Interpretation of the results is complex, and the overall 11% difference is caused by several factors (not simply coupling of the two phases). From their work, it appears that vapour flow alone is not particularly important; however, inclusion of heat transfer due to the bulk movement of liquid can influence the results by approximately 5%.

Material properties

In this work, the water retention curve is expressed as a natural logarithmic function according to (Thomas *et al.*, 1994)

$$S_r = 1 - \frac{5}{37}\ln\left(\frac{-P_w}{100}\right) \tag{14}$$

where P_w is pore water pressure. This relationship, together with the equilibrium condition for a given depth of water table, defines the degree of saturation variation with depth.

Table 4. Soil properties used in the calculation of thermal conductivity

Parameter	Value
Porosity, η	0·37
Solid phase thermal conductivity, λ_s: W/m K	4·0
Water phase thermal conductivity, λ_s: W/m K	0·573
Air phase thermal conductivity, λ_a: W/m K	0·12

Application of the geometric mean approach (equations (9) to (12)), using the constants shown in Table 4, yields the variation of thermal conductivity with depth for each simulation.

Numerical investigation

The analysed domains for both one-dimensional and the two-dimensional test problems considered are shown in Figs 13(a) and 13(b) respectively. In both cases a series of steady-state heat conduction simulations have been performed using thermal properties that take into account the position of the water table, and hence also take into account the dependence of thermal conductivity on water content. The (arbitrary) depth variation of water table considered is also shown in Fig. 13.

The first test problem considered is a one-dimensional heat conduction problem. In practice, the assumption of unidirectional heat flow appears adequate for a number of cases. For example, heat flow directly beneath large ground floor areas, where the external climatic influence and boundary effects are relatively minor, is likely to be predominantly

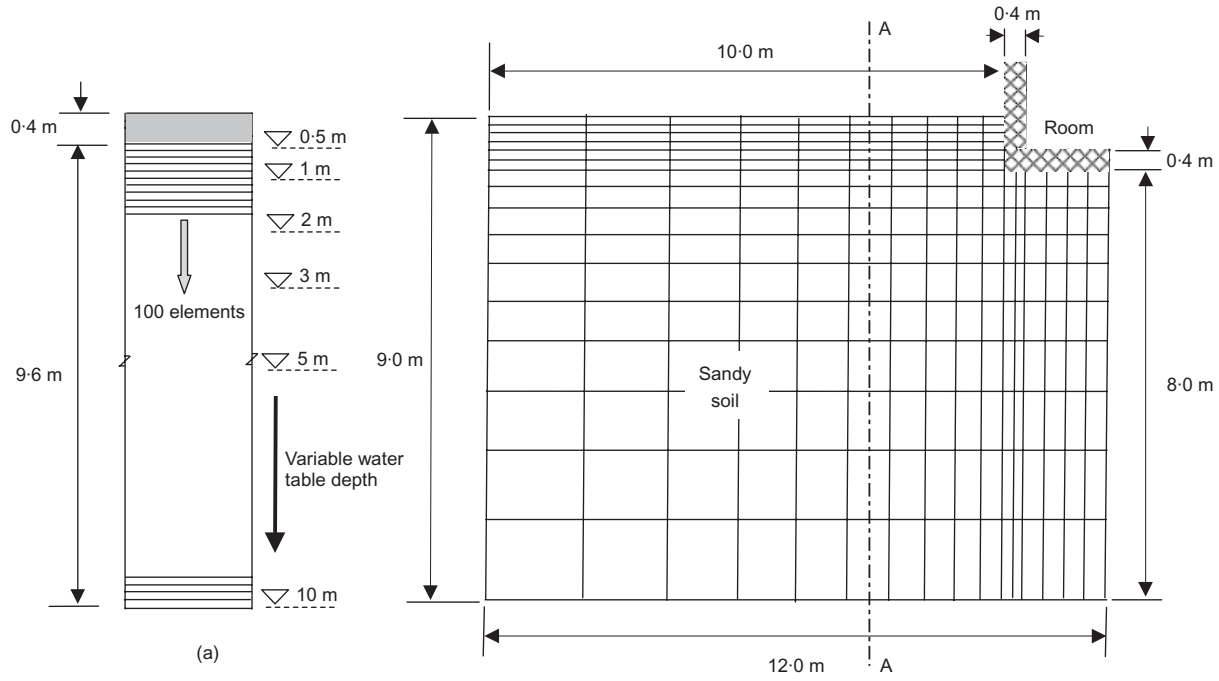

Fig. 13. (a) One-dimensional and (b) two-dimensional test problems

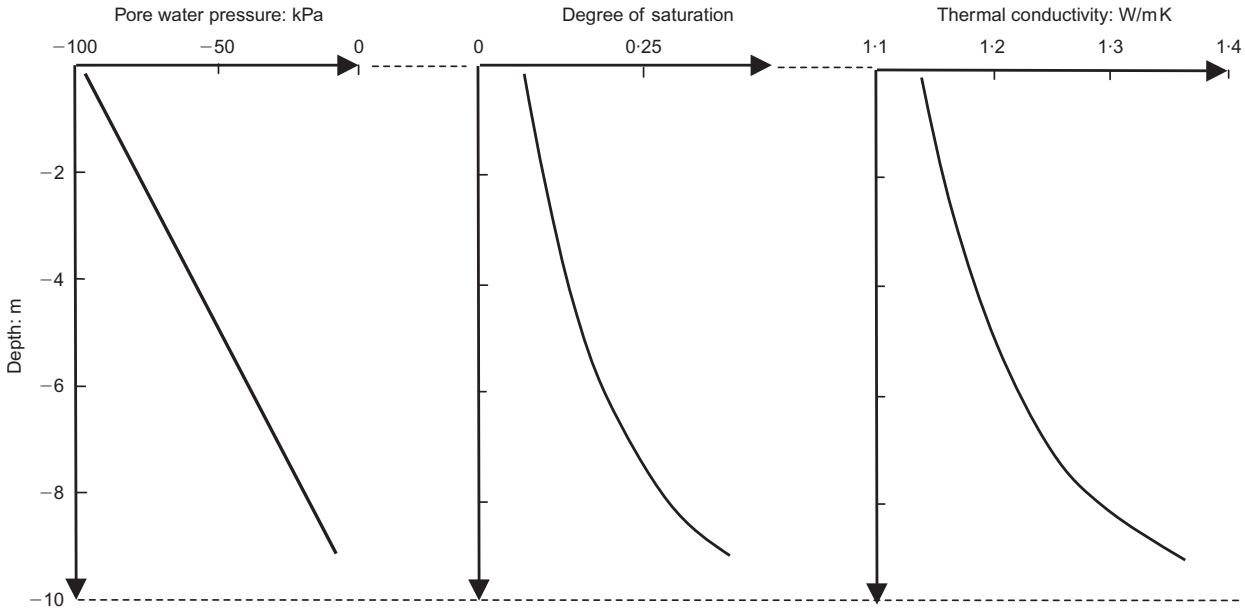

Fig. 14. Typical depth variation of hydraulic and thermal properties

one-dimensional. The mesh extends to a depth of 10 m below finished floor level, with a concrete floor of 0·40 m thickness. The concrete is assumed to have a thermal conductivity of 1·37 W/m K (Rees *et al.*, 1995). The soil is assumed to be homogeneous and isotropic, with a porosity of 0·37. Based on previous work (Thomas & Rees, 1998), the temperature at the bottom boundary is fixed at 13·5°C. It is recognised that this value may vary slightly from location to location, but its precise magnitude is not of particular significance in an exercise of this nature. The surface temperature (room temperature) is fixed at 20°C. Steady-state heat conduction simulations of this problem have then been computed for water table depths of 10 m, 5 m, 3 m, 2 m, 1 m and 0·5 m below the surface level.

For example, a water table depth of 10 m yields the pore water pressure distribution (in gravitational equilibrium) shown in Fig. 14. The corresponding depth variation of the degree of saturation and the thermal conductivity are also shown in Fig. 14. It is assumed that no flow of water occurs.

The results achieved from the set of one-dimensional analyses are summarised in Fig. 15(a). In particular, the variation of heat flux at the surface is plotted against the depth of the groundwater table. The results show that the heat loss to the ground increases almost linearly as the groundwater table rises. A maximum increase in heat flux of 60% was calculated.

The two-dimensional test problem uses the same logic applied above, but now to explore the response a typical shallow earth-contact structure. The material properties, room temperature and lower boundary temperature are the same as those used in the one-dimensional problem. In order to illustrate the significance of the problem at a time of high energy demand, the outside temperature is set at a typical average daily winter temperature for the UK, 3·5°C (Thomas & Rees, 1998). The vertical boundaries are both adiabatic (one is an axis of symmetry; the other is remote from the building). Thus a clear two-dimensional heat transfer pattern is imposed.

The two-dimensional problem has also been analysed to obtain a steady-state temperature solution for the same range of groundwater table depths as above. In this case the results are presented in terms of the total heat flux across the earth-contact region of the domain (wall plus floor). The results are shown in Fig. 15(b), where it can be seen that once again the heat loss to the ground increases significantly as the water table rises. A 23% variation in computed values has occurred. The depth variation of properties at section A–A (Fig. 13) was found to be very similar to the results shown in Fig. 14 for the one-dimensional problem.

Typical steady-state temperature distributions for both the one-dimensional and two-dimensional problems are shown in Fig. 16. It was found that the steady-state temperature distribution in both cases was not significantly influenced by the variation in water table depth.

Therefore the results reveal that construction programmes that may cause a rise in groundwater table, such as tidal barrage schemes, may have a significant influence on the energy efficiency of buildings. The results indicate the importance of considering soil moisture content when estimating soil thermal conductivity.

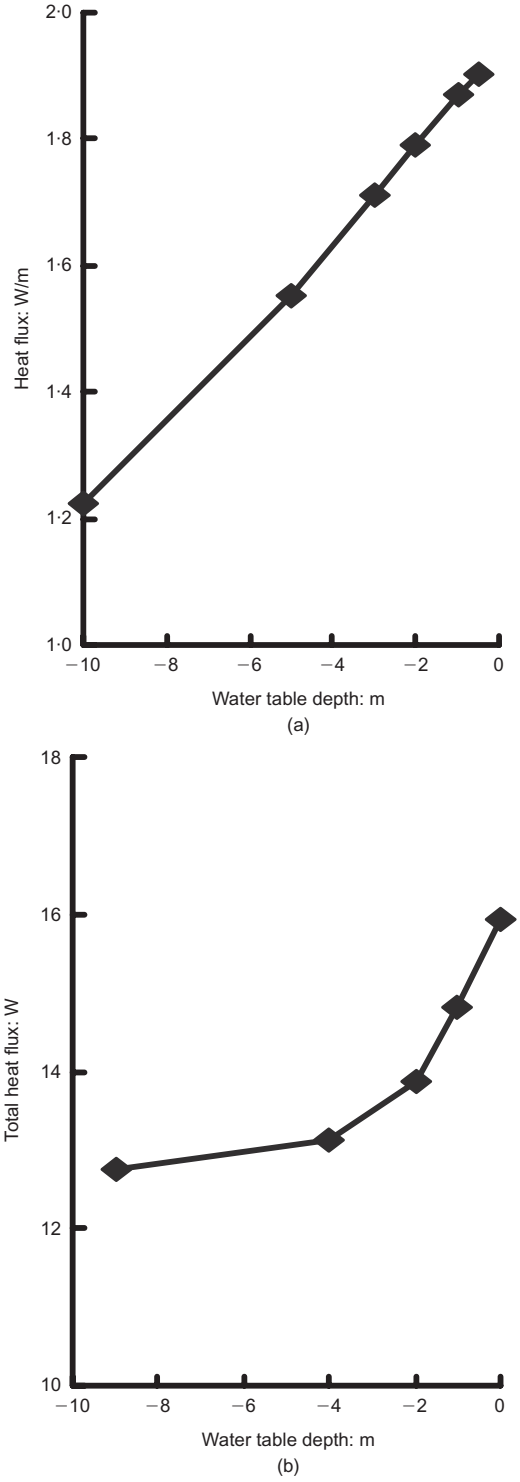

Fig. 15. Influence of water table depth on heat flux: (a) one-dimensional test problem; (b) two-dimensional test problem

CONCLUSIONS

The results of two case studies involving the direct measurement of ground heat transfer beneath full-scale buildings have been presented. The first experiment was conducted at the site of a modern commercial building at Cardiff University; the second was carried out (by others) at Sendai University, Japan. The measured data from both experimental sites have been used to assess the performance of a numerical ground heat transfer model. Overall, the approach developed has been shown to be capable of representing seasonal trends in ground heat transfer beneath and adjacent to real buildings. Results have been presented that show good correlation between experiments and simulations. The paper also shows that the thermal properties of soil can be adequately estimated using the geometric mean approach.

The influence of varying ground moisture content beneath buildings on heat loss through ground floor slabs has also

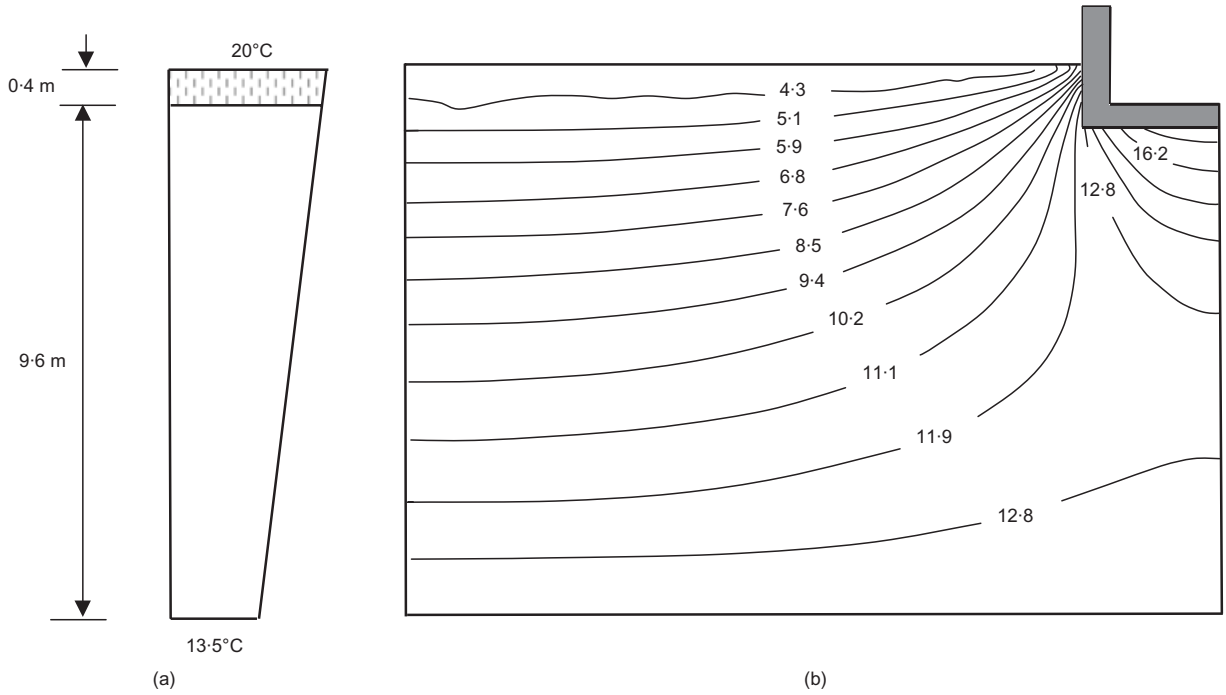

Fig. 16. (a) One-dimensional and (b) two-dimensional steady-state temperature distribution (°C)

been considered. The results of two test-case simulations show that significant differences in calculated heat loss occur as the depth of the groundwater table changes. Attention has been focused on providing an assessment of the significance of the variation of thermal conductivity with soil moisture content. The work is undertaken for conditions of static moisture content distributions. A 60% increase in heat flux was obtained from a one-dimensional problem, and a 20% increase for a two-dimensional shallow structure. The results provide an indication of the significance of this particular aspect of the ground heat transfer problem. The work should be considered separately from other work on ground flow beneath the water table.

NOTATION

C	volumetric heat capacity
c	specific heat capacity
N_i, N_j	shape functions
$\boldsymbol{q}$	heat flux
S_r	degree of saturation
T	temperature
x, z	coordinates
Γ	boundary
η	porosity
λ	thermal conductivity
Π	product summation
π	heat flux at boundary
ρ	density
χ	volume fraction
Ω	domain

REFERENCES

Adjali, M. H, Davies, M. & Rees, S. W. (2004). A comparative study of design guide calculations and measured heat loss through the ground. *Build. Environ.* **39**, No. 11, 1301–1311.

AICVF (Association des Ingénieurs de Climatisation et de Ventilation de France) (1990). *AICVF Guide: Chauffage: Calculs des déperditions et charges thermiques d'hiver*. Paris: Pyc Edition.

Al-Ajmi, F., Loveday, D. L. & Hanby, V. I. (2006). The cooling potential of earth–air heat exchangers for domestic buildings in a desert climate. *Build. Environ.* **41**, No. 3, 235–244.

ASHRAE (1993) *ASHRAE handbook of fundamentals*. Atlanta, GA: American Society of Heating, Refrigerating and Air-conditioning Engineers.

Banfill, P. F. G. & Peacock, A. D. (2007). Energy-efficient new housing: the UK reaches for sustainability. *Build. Res. Inform.* **35**, No. 4, 426–436.

Bloomer, J. R. (1981). Thermal conductivities of mudrocks in the United Kingdom. *Q. J. Engng Geol.* **14**, No. 4, 357–362.

Brandl, H. (2006). Energy foundations and other thermo-active ground structures. *Géotechnique* **56**, No. 2, 81–122.

CEC (2006). *Action plan for energy efficiency: Realising the potential*, COM(2006)545 final. Brussels: Commission of the European Communities.

CEN (1992). *Thermal performance of buildings: Heat exchange with the ground: Calculation method*, CEN/TC 89. Brussels: European Committee for Standardisation.

CIBSE (1986). *Guide A3: Thermal properties of building structures*. London: Chartered Institution of Building Services Engineers.

Cui, Y. J., Lu, Y. F., Delage, P. & Riffard, M. (2005). Field simulation of in situ water content and temperature changes due to ground–atmospheric interactions. *Géotechnique* **55**, No. 7, 557–567.

Defra (2006). Climate change: The UK programme 2006, CM6764 SE/2006/43. London: The Stationery Office.

De Vries, D. A. (1966). Thermal properties of soils. In *Physics of the plant environment* (ed. W. R. Van Wijk), pp. 210–233. Amsterdam: North-Holland.

Farouki, O. (1982). *Evaluation of methods for calculating soil thermal conductivity*, CRREL Report 82-8. Hanover, NH: Cold Regions Research and Engineering Laboratory, US Army Corps of Engineers.

Hasegawa, F., Yoshino, H. & Matsumoto, S. (1987). Optimum use of solar energy techniques in a semi-underground house: first year measurement and computer analysis. *Tunnelling Underground Space Technol.* **2**, No. 4, 429–435.

IPCC (2007). *Climate change 2007: The physical science basis*, Fourth Assessment Report of the Intergovernmental Panel on Climate Change. Geneva: IPCC.

Janssen, H., Carmeliet, J. & Hens, H. (2004). The influence of soil moisture transfer on building heat loss via the ground. *Build. Environ.* **39**, No. 7, 825–836.

Krarti, M. (2004a). Analysis of heat and moisture transfer beneath freezer foundations: Part I. *Trans. ASME J. Solar Energy Engng* **126**, No. 2, 716–725.

Krarti, M. (2004b). Analysis of heat and moisture transfer beneath

freezer foundations: Part II. *Trans. ASME J. Solar Energy Engng* **126**, No. 2, 726–731.

Kumar, R., Sachdeva, S. & Kaushik, S. C. (2007). Dynamic earth-contact building: a sustainable low-energy technology. *Build. Environ.* **42**, No. 6, 2450–2460.

Lewis, R. W., Morgan, K., Thomas, H. R. & Seetharamu, K. N. (1996). *The finite element method in heat transfer analysis*. Chichester: Wiley.

Lowe, R. (2007). Editorial: Addressing the challenges of climate change for the built environment. *Build. Res. Inform.* **35**, No. 4, 343–350.

Meacham, B., Bowen, R., Traw, J. & Moore, A. (2005). Performance-based building regulation: current situation and future needs. *Build. Res. Inform.* **33**, No. 2, 91–106.

Rees, S. W. & Thomas, H. R. (1997). *A numerical and experimental study of heat and moisture transfer from earth-contact structures*. EPSRC Grant GR/K77471.

Rees, S. W., Adjali, M. H., Zhou, Z., Davies, M. & Thomas, H. R. (2000). Ground heat transfer effects on the thermal performance of earth-contact structures. *J. Renewable Sustainable Energy Rev.* **4**, No. 3, 213–265.

Rees, S. W., Lloyd, R. M. & Thomas, H. R. (1995). A numerical simulation of measured transient heat transfer through a concrete ground floor slab and underlying substrata. *Int. J. Numer. Heat Fluid Flow* **5**, 669–683.

Sass, J. H., Lachenbruch, A. H. & Munroe, R. J. (1971). Thermal conductivity of rocks from measurements on fragments and its application to heat-flow determinations. *J. Geophys. Res.* **76**, No. 14, 3391–3401.

Sobotka, P., Yoshino, H. & Matsumoto, S. (1995). The analysis of deep basement heat loss by measurements and calculations. *ASHRAE Trans.* **101**, No. 2, 186–197.

Stern, N. (2006). *The economics of climate change*. Cambridge: Cambridge University Press.

Tang, A. M., Cui, Y. J. & Le, T. T. (2008). A study on the thermal conductivity of compacted bentonites. *Appl. Clay Sci.* **41**, Nos. 3–4, 188–189.

Thomas, H. R. & Rees, S. W. (1998). The thermal performance of ground floor slabs: a full scale in-situ experiment. *Build. Environ.* **34**, No. 2, 139–164.

Thomas, H. R., He, Y., Ramesh, A., Zhou, Z., Villar, M. V. & Cuevas, J. (1994). Heating unsaturated soil: an experimental and numerical investigation. *Proc. 3rd Eur. Conf. Numer. Methods in Geotech. Engng, Manchester*, 181–186.

Underwood, C. P. (2007). Analysis of vertical ground loop heat exchangers applied to buildings in the UK. *Build. Serv. Eng. Res. Technol.* **28**, No. 2, 133–159.

Woodside, W. & Messmer, J. H. (1961). Thermal conductivity of porous media. *J. Appl. Phys.* **32**, No. 9, 1688–1706.

Yoshino, H., Matsumoto, S., Hasegawa, F. & Nagatomo, M. (1990). Effects of thermal insulation located in the earth around a semi-underground room: computer analysis by the finite element method. *ASHRAE Trans.* **96**, No. 1, 103–111.

Yoshino, H., Matsumoto, S., Nagatomo, M. & Sakanishi, T. (1992). Five-year measurement of thermal performance for a semi-underground test house. *Tunnelling Underground Space Technol.* **7**, No. 4, 339–346.

Zhong, Z, & Braun, J. E. (2007). A simple method for estimating transient heat transfer in slab-on-ground floors. *Build. Environ.* **42**, No. 3, 1071–1080.